Large magnetic entropy change and adiabatic temperature rise of a $Gd_{55}Al_{20}Co_{20}Ni_5$ bulk metallic glass

Cite as: J. Appl. Phys. **115**, 223904 (2014); https://doi.org/10.1063/1.4882735
Submitted: 24 December 2013 . Accepted: 29 May 2014 . Published Online: 10 June 2014

L. Xia, M. B. Tang, K. C. Chan, and Y. D. Dong

Large magnetic entropy change and adiabatic temperature rise of a $Gd_{55}Al_{20}Co_{20}Ni_5$ bulk metallic glass

L. Xia,[1,2,a)] M. B. Tang,[3] K. C. Chan,[2] and Y. D. Dong[1]
[1]*Key Laboratory for Microstructure & Institute of Materials, Shanghai University, Shanghai 200072, China*
[2]*Department of Industrial and Systems Engineering, The Hong Kong Polytechnic University, Hung Hom, Hong Kong*
[3]*Shanghai Institute of Ceramics, Chinese Academy of Science, Shanghai 200050, China*

(Received 24 December 2013; accepted 29 May 2014; published online 10 June 2014)

$Gd_{55}Al_{20}Co_{20}Ni_5$ bulk metallic glass (BMG) was synthesized by minor Ni substitution for Co in the $Gd_{55}Al_{20}Co_{25}$ BMG in which excellent glass forming ability (GFA) and magneto-caloric effect were reported previously. The $Gd_{55}Al_{20}Ni_{20}Co_5$ amorphous rod has a similar GFA to the $Gd_{55}Al_{20}Co_{25}$ BMG but exhibits better magnetic properties. The peak value of magnetic entropy change ($-\Delta S_m^{peak}$) of the $Gd_{55}Al_{20}Co_{20}Ni_5$ BMG is 9.8 Jkg^{-1} K^{-1}. The field dependence of $-\Delta S_m^{peak}$ follows a $-\Delta S_m^{peak} \propto H^{0.85}$ relationship. The adiabatic temperature rise of the rod is 4.74 K under 5 T and is larger than of other BMGs previously reported. The improved magnetic properties were supposed to be induced by the enhanced interaction between 4f electron in the rare-earth and 3d electron in the transition metal elements by means of a minor Ni substitution for Co. © *2014 AIP Publishing LLC*. [http://dx.doi.org/10.1063/1.4882735]

I. INTRODUCTION

The heating or cooling of magnetic materials under a variable magnetic field, known as the magnetocaloric effect (MCE), was firstly discovered in 1881 by Warburg.[1,2] Materials with giant MCE have attracted tremendous interest since their first discovery in 1997, because magnetic refrigeration techniques based on MCE are regarded as more energy efficient and environmentally friendly techniques than the traditional vapor-cycle refrigeration.[2–10] As a result, a lot of materials with excellent MCE have been fabricated in the past two decades.

According to the type of phase transition they undergo at the ordering temperature, magnetic refrigerant materials can be classified into two types. Most of the crystalline alloys, including Mn-Fe-P-As,[10] Gd-Si-Ge,[11,12] La-Fe-Si,[13,14] Ni-Mn-Ga,[15] Mn-As-Sb,[16,17] and their hybrids, undergo a first-order magnetic phase transition and exhibit a sharp magnetic entropy change (ΔS_m) peak, as well as large adiabatic temperature change in a refrigeration cycle. In contrast, amorphous alloys and a few crystalline alloys (such as Gd and $Gd_6Co_2Si_3$) undergo a reversible second-order magnetic transition and exhibit a broad distribution of the ΔS_m peak.[18–31] Although the peak values of ΔS_m (ΔS_m^{peak}) for Gd, $Gd_6Co_2Si_3$ and the amorphous alloys are not as high as those of the first type alloys, the second type alloys, especially the amorphous alloys, exhibit much higher refrigeration capacity (RC) than the first type alloys due to their broadened ΔS_m peak.[20–31] Additionally, the amorphous alloys show some further characteristics that are superior to the crystalline alloys, such as low energy loss due to nearly zero magnetic hysteresis and large electric resistance, high corrosion resistance, and fine molding/processing behavior. The low hysteresis loss as well as high RC, which is very important in regard to the high efficiency of magnetic refrigeration, makes the amorphous alloys more suitable candidates for application as magnetic refrigerants.[2–31] Therefore, one of the new challenges in the field of magnetic refrigeration is to improve the ΔS_m^{peak} of amorphous alloys to be as high as possible.

On the other hand, unlike the situation in intermetallic compounds, the tunable physical properties can be easily obtained by continuous composition variation in the amorphous alloys. As a matter of fact, element substitution or minor addition of other elements is a useful way for the improvement of glass forming ability (GFA), physical and mechanical properties of the amorphous alloys. In this work, based on our recent results on $Gd_{55}Al_{20}Co_{25}$ bulk metallic glass (BMG) which has excellent GFA and large magnetic entropy change,[25] we try to further enhance the magnetic properties by element substitution of the $Gd_{55}Al_{20}Co_{25}$ BMG. A $Gd_{55}Al_{20}Co_{20}Ni_5$ bulk sample with fully amorphous features was prepared by the conventional copper mold suction casting method. The effect of Ni substitution for Co on the GFA and magnetic properties of $Gd_{55}Al_{20}Co_{25}$ BMG was investigated.

II. EXPERIMENTS

Ingots with nominal compositions of $Gd_{55}Al_{20}Co_{20}Ni_5$ and $Gd_{55}Al_{20}Co_{25}$ were prepared by arc-melting 99.9% (at. %) pure Gd, Co, Ni, and Al under a titanium-gettered argon atmosphere, respectively. The as-cast rods of diameter 2 mm were prepared by a copper mold suction casting method under the protection of an argon atmosphere. The amorphicity of the two samples was confirmed by X-ray diffraction (XRD) on a Rigaku D\max-2550 diffractometer using Cu K_α radiation. The thermal properties of the BMGs were measured by a Perkin-Elmer DIAMOND differential scanning calorimetry (DSC) under a purified argon atmosphere at a heating rate of 20 K/min. The melting and liquidus temperatures of

a)Author to whom correspondence should be addressed. Electronic addresses: xialei@shu.edu.cn

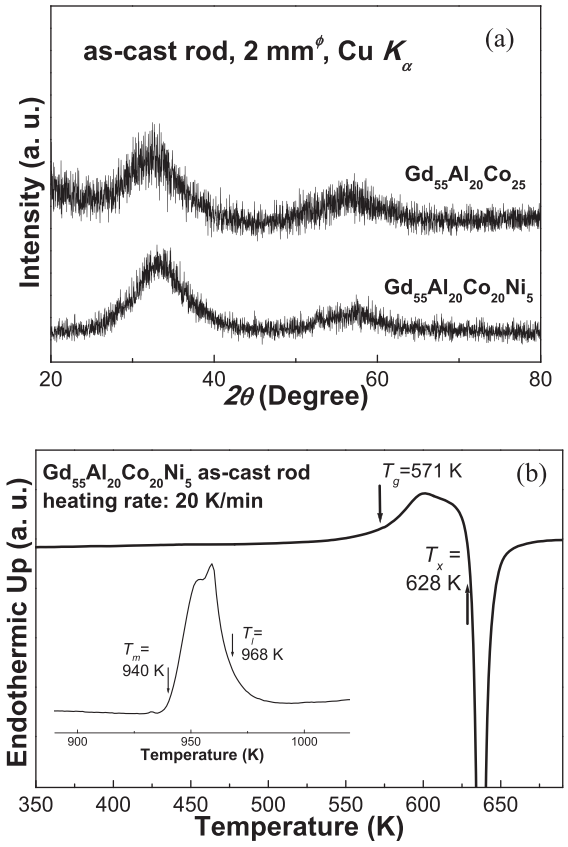

FIG. 1. (a) XRD patterns of the $Gd_{55}Al_{20}Co_{20}Ni_5$ and $Gd_{55}Al_{20}Co_{25}$ as-cast rods; (b) the DSC trace of $Gd_{55}Al_{20}Co_{20}Ni_5$ as-cast rod at a heating rate of 20 K/min, the inset shows the melting behavior of the rod.

the samples were obtained from the high temperature DSC (HTDSC) curve measured by a NETZSCH 404C DSC at the same heating rate. The magnetic properties of the BMGs, including the magnetic hysteresis loops and the magnetization curve (the *M-H* curve, where *M* is the magnetization of the sample under a magnetic field *H*) under a field of 5 T, the temperature dependence magnetization curve (the *M-T* curve, where *T* is the temperature) under a field of 300 Oe, were measured from 10 K to 300 K by a Quantum Design Physical Properties Measurement System (PPMS 6000).

III. RESULTS AND DISCUSSION

Figure 1(a) shows the XRD patterns of the $Gd_{55}Al_{20}Co_{20}Ni_5$ and $Gd_{55}Al_{20}Co_{25}$ as-cast rods of a diameter around 2 mm. The typical broad diffraction maxima of the amorphous phases in the XRD patterns illustrate the glassy nature of both samples. DSC traces of the $Gd_{55}Al_{20}Co_{25}$ and the $Gd_{55}Al_{20}Co_{20}Ni_5$ as-cast rods are shown in Fig. 1(b), where the inset is the HTDSC curve of the rod. The endothermic glass transition behavior before crystallization in the continuous DSC trace also indicates the amorphous characteristics of the as-cast rod. The onset temperatures of glass transition (T_g) and the crystallization (T_x) at a heating rate of 20 K/min are about 571 K and 628 K, as marked respectively on the continuous DSC trace. The melting and liquidus temperatures (T_m and T_l) obtained from the HTDSC curve are about 940 K and 968 K, also marked clearly in the inset of Fig. 1(b). The supercooled liquid region ΔT_x ($= T_x - T_g$) and the reduced glass transition temperature T_{rg} ($= T_g/T_l$) are about 57 K and 0.59, respectively. Compared to the thermal properties of the $Gd_{55}Al_{20}Co_{25}$ BMG, as listed in Table I, it is found that the minor Ni substitution for Co slightly improve the T_{rg} but decrease the ΔT_x.

Figure 2(a) shows the hysteresis loops of the $Gd_{55}Al_{20}Co_{20}Ni_5$ as-cast rod, measured at 10 K and 300 K, under a field of 2 T. The $Gd_{55}Al_{20}Co_{20}Ni_5$ glassy rod is paramagnetic at 300 K and is ferromagnetic at 10 K and the saturation magnetization (M_s) of the $Gd_{55}Al_{20}Co_{20}Ni_5$ as-cast rod is 217 Am^2/kg, which is about 5% higher than the M_s of the as-cast $Gd_{55}Al_{20}Co_{25}$ rod at the same temperature (10 K). The higher M_s value suggests a higher magnetic entropy change of the $Gd_{55}Al_{20}Co_{20}Ni_5$ as-cast rod due to the enlarged total magnetic moment by element substitution. The coercivity of the $Gd_{55}Al_{20}Co_{20}Ni_5$ as-cast rod is nearly zero (~2.8 kA/m), as-shown in the details of the heteresis loop measured at 10 K in the inset of Fig. 2(a). The *M-T* curves for the $Gd_{55}Al_{20}Co_{20}Ni_5$ and $Gd_{55}Al_{20}Co_{25}$ as-cast rods under a field of 300 Oe from 10 K to 300 K are shown in Fig. 2(b). The Curie temperature (T_c) of the $Gd_{55}Al_{20}Co_{20}Ni_5$ BMG is 105 K and is about 7 K lower than that of the $Gd_{55}Al_{20}Co_{25}$ BMG, indicating a lower peak temperature of ΔS_m for the $Gd_{55}Al_{20}Co_{20}Ni_5$ BMG.

The isothermal *M-H* curves of the $Gd_{55}Al_{20}Co_{20}Ni_5$ glassy rod measured at temperatures ranging from 20 K to 160 K under a magnetic field of 5 T are shown in the Fig. 3(a). By applying the thermodynamic Maxwell equation, the temperature dependence of ΔS_m ($\Delta S_m - T$ curve) under a field of 3979 kA/m for both the $Gd_{55}Al_{20}Co_{20}Ni_5$ and $Gd_{55}Al_{20}Co_{25}$ glassy rods can be constructed as follows:

$$\Delta S_m(T,H) = S_m(T,H) - S_m(T,0) = \int_0^H \left(\frac{\partial M}{\partial T}\right)_H dH. \quad (1)$$

Figure 3(b) shows the $\Delta S_m - T$ curves for the $Gd_{55}Al_{20}Co_{20}Ni_5$ as well as the $Gd_{55}Al_{20}Co_{25}$ glassy rods. The BMGs exhibit typical broadened ΔS_m peaks of ferromagnets with second order phase transition. ΔS_m^{peak} of the

TABLE I. The thermal properties and magnetic properties of the $Gd_{55}Al_{20}Co_{20}Ni_5$ and $Gd_{55}Al_{20}Co_{25}$ BMGs.

	T_g (K)	T_x (K)	T_l (K)	T_m (K)	ΔT_x (K)	T_{rg}
$Gd_{55}Al_{20}Co_{20}Ni_5$	571	628	968	940	57	0.59
$Gd_{55}Al_{20}Co_{25}$	563	629	972	936	66	0.58
	T_c (K)	M_s (Am^2/kg) under 2 T	$-\Delta S_m^{peak}$ ($Jkg^{-1}K^{-1}$) under 5 T	RC_{HHW} (Jkg^{-1}) under 5 T	RC_A (Jkg^{-1}) under 5 T	
$Gd_{55}Al_{20}Co_{20}Ni_5$	105	217	9.8	615	827	
$Gd_{55}Al_{20}Co_{25}$	112	206.5	9	608	800	

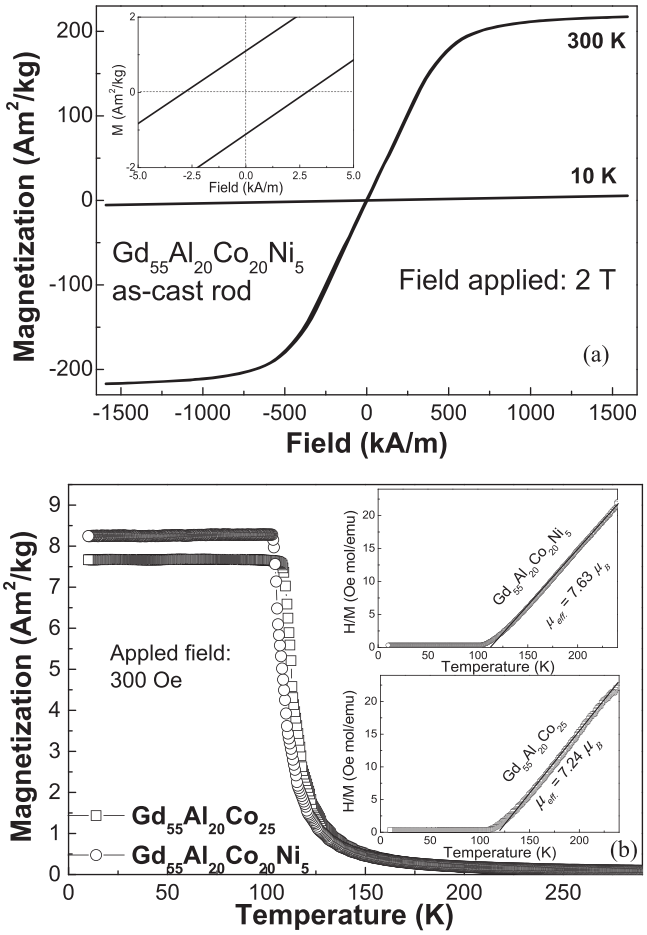

FIG. 2. (a) Magnetic hysteresis loops of the $Gd_{55}Al_{20}Co_{20}Ni_5$ as-cast rod at 300 K and 10 K under a magnetic field of 2 T, the inset the details of the hysteresis; (b) the *M-T* curves of the $Gd_{55}Al_{20}Co_{20}Ni_5$ and $Gd_{55}Al_{20}Co_{25}$ as-cast rods under the field of 300 Oe, the inset shows the *H/M-T* curves and their Curie-Weiss fitting for the as-cast rods.

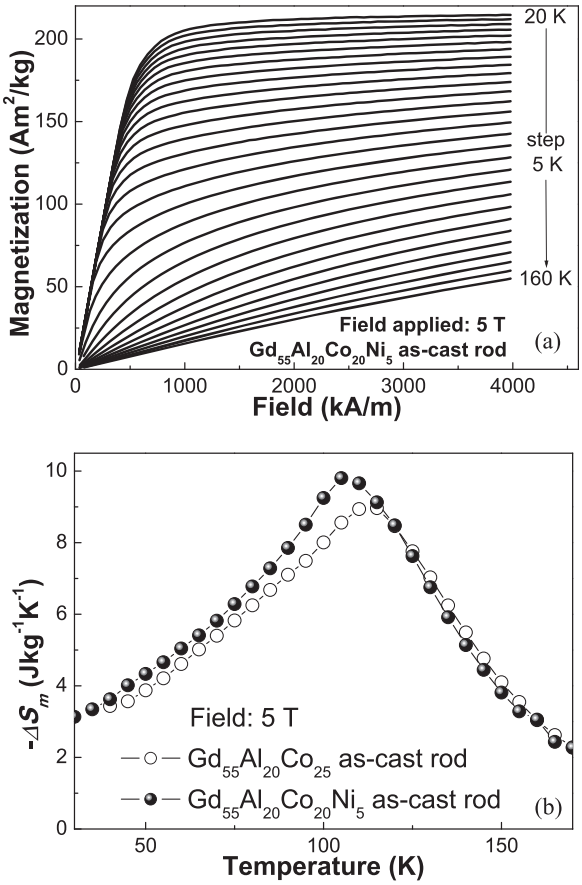

FIG. 3. (a) Isothermal magnetization curves of the $Gd_{55}Al_{20}Co_{20}Ni_5$ as-cast rod under a magnetic field of 5 T; (b) $(-\Delta S_m)$-*T* curves of the $Gd_{55}Al_{20}Co_{20}Ni_5$ and $Gd_{55}Al_{20}Co_{25}$ as-cast rods under 5 T.

as-cast $Gd_{55}Al_{20}Co_{20}Ni_5$ rod under a magnetic field of 5 T reaches to a rather high value up to 9.8 $Jkg^{-1}K^{-1}$ at 105 K (about 71 $mJcm^{-3}K^{-1}$, where the density of the alloy is estimated to be about 7.3 g/cm^3), which is about 9% higher than the ΔS_m^{peak} ($=9$ $Jkg^{-1}K^{-1}$ at 112 K) of the $Gd_{55}Al_{20}Co_{25}$ glassy rod.

Figure 4(a) shows the $\Delta S_m - T$ curves for the $Gd_{55}Al_{20}Co_{20}Ni_5$ under different magnetic fields. The $-\Delta S_m^{peak}$ obtained under 796 kA/m, 1592 kA/m, 2387 kA/m, 3183 kA/m, and 3979 kA/m are about 2.47 $Jkg^{-1}K^{-1}$, 4.7 $Jkg^{-1}K^{-1}$, 6.59 $Jkg^{-1}K^{-1}$, 8.27 $Jkg^{-1}K^{-1}$, and 9.8 $Jkg^{-1}K^{-1}$ at 105 K, respectively. The field dependence of $-\Delta S_m^{peak}$ of the $Gd_{55}Al_{20}Co_{20}Ni_5$ as-cast rod is roughly in accordance with the $-\Delta S_m^{peak} \propto H^n$ relationship for the amorphous alloys with second order magnetic phase transition behavior at the temperature near T_c.[32] Based on the experimental $\ln(-\Delta S_m^{peak})$ vs $\ln(H)$ plots of the rod, as shown in Fig. 4(b), the n value is found to be 0.85. The critical exponents, which are closely related to n, can be derived from the dc magnetization curves using the Kouvel-Fisher method. By constructing the Arrott-Noakes (A-N) plots, we can obtain $\beta = 0.482$ and $\gamma = 0.956$, as shown in the inset of Fig. 4(b). The values of the critical exponents are very close to those predicted by the mean field model. The linear fitting of the isothermal $(-\Delta S_m)$ vs M^2 plots, as shown in Fig. 4(c), also suggests that the magnetic behaviors of the BMG can be well described by the mean field theory.[34] However, the n value at T_c calculated by $n(T = T_c) = 1 + (\beta - 1)/(\beta + \gamma)$ is significantly different from the one obtained from the $-\Delta S_m^{peak}$-*H* curve of the $Gd_{55}Al_{20}Co_{20}Ni_5$ bulk amorphous sample, which is considered to be due to the microstructure of the BMGs being much more complicated than that of a single phase alloy because of the presence of short-range order (SRO), medium range order (MRO) or even nano-crystallized (NC) structures embedded in the disordered matrix.[32,33,35,36] These structures may affect the n value of the BMGs because it is regarded that n is field independent at Curie temperature for a single phase material but it will change with the magnetic field at any temperatures for a multiphase material. By carefully examining the $d[\ln -\Delta S_m^{peak})]/d[\ln(H)]$ data plots, we have found that the instantaneous slope of the $\ln(-\Delta S_m^{peak})$-$\ln(H)$ curve decreases continuously from about 0.956 under 1 T to about 0.756 under 5 T. The n value is very close to 0.75 under 5 T but becomes larger with a decreased magnetic field. It is considered that the presence of the SRO, MRO, or NC structures may obstruct the magnetization of the rod, leading to the reduction of $-\Delta S_m^{peak}$ at low magnetic field. However, more work is needed to further understand the effect of these structures on the n value as well as the critical exponents.

For ferromagnets with a broadened but less intense ΔS_m peak, RC is regarded as a more important parameter from

the technological point of view rather than the ΔS_m^{peak} for evaluating the MCE of magnetic refrigerants, because the RC not only considers the ΔS_m^{peak} but also takes into account the shape of the $\Delta S_m - T$ curve of the refrigerant materials. The RC of the samples, defined as the amount of heat that can be transferred in one thermodynamic cycle, is usually calculated in two ways as follows:

$$RC_{HHW} = -\Delta S_m^{peak} \times \Delta T_m, \tag{2}$$

where ΔT_m is the temperature width at the half maximum of ΔS_m^{peak}; and

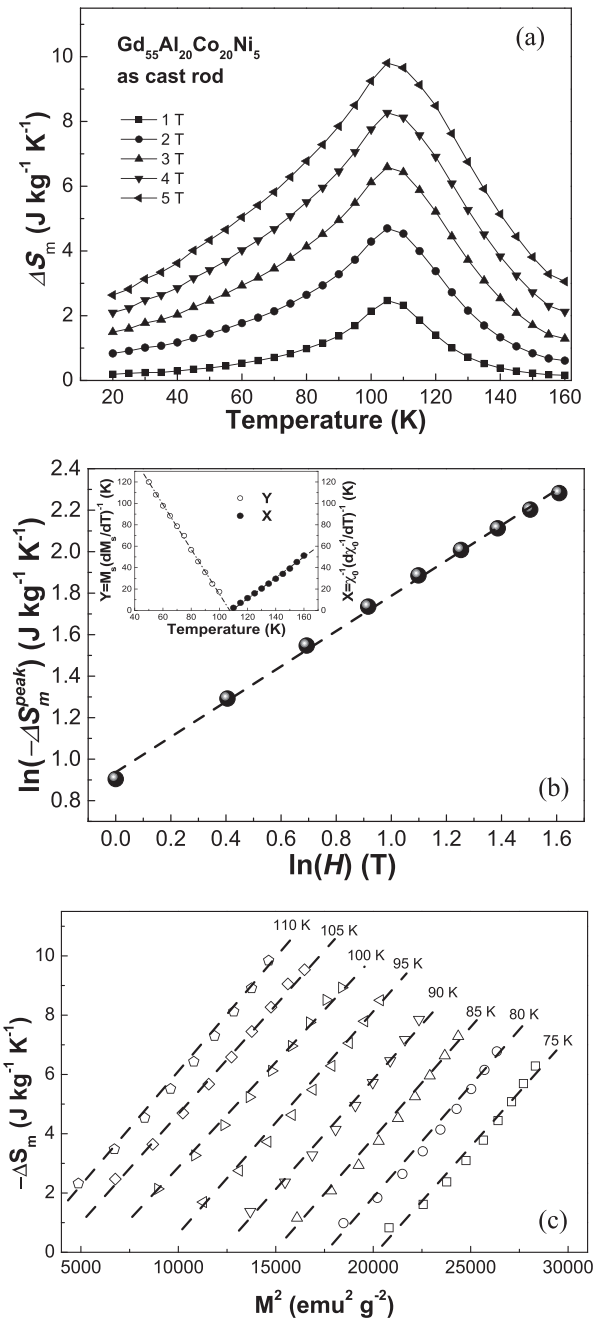

FIG. 4. (a) The $(-\Delta S_m)$-T curves of the $Gd_{55}Al_{20}Co_{20}Ni_5$ under the field of 1 T, 2 T, 3 T, 4 T, and 5 T; (b) the $\ln(-\Delta S_m^{peak})$ vs $\ln(H)$ plots of the $Gd_{55}Al_{20}Co_{20}Ni_5$ as-cast rod, the inset shows the Kouvel-Fisher construction for determining the critical exponents; (c) Isothermal $(-\Delta S_m)$ vs M^2 curves for the $Gd_{55}Al_{20}Co_{20}Ni_5$ BMG, dash lines are linear fits to data.

$$RC_A = \int_{T_1}^{T_2} (-\Delta S_m(T,H))dT, \tag{3}$$

where T_1 and T_2 are the onset and offset temperature of ΔT_m.

The RC of the $Gd_{55}Al_{20}Co_{20}Ni_5$ as-cast rod calculated according to Eqs. (2) and (3) is about 615 Jkg^{-1} and 829 Jkg^{-1} under 5 T, respectively, as listed in Table I. For comparison purposes, the RC_{HHW} and RC_A of $Gd_{55}Al_{20}Co_{25}$ as-cast rod are also listed in Table I. Both the values of the $Gd_{55}Al_{20}Co_{20}Ni_5$ BMG are higher than those of the $Gd_{55}Al_{20}Co_{25}$ BMG, indicating an enhanced refrigeration efficiency by minor Ni addition. Furthermore, the RC of the $Gd_{55}Al_{20}Co_{20}Ni_5$ as-cast rod is higher than most of the BMGs reported previously, and much higher than the intermetallic compounds, making the $Gd_{55}Al_{20}Co_{20}Ni_5$ BMG an attractive candidate for magnetic refrigeration.[2–31]

A more direct way for a comparison between different magneto-caloric materials is the adiabatic temperature rise (ΔT_{ad}) under a certain magnetic field. ΔT_{ad} as a function of temperature ($\Delta T_{ad} - T$ curve) under a magnetic field can be determined directly from the isentropic difference between the total entropy under a zero field and a certain magnetic field; or indirectly from the measured magnetization and the temperature dependence of $C_0(T)$ as follows:

$$\Delta T_{ad}(T, 0 \rightarrow H) = -\frac{T}{C_0(T)} \Delta S_m(T, 0 \rightarrow H). \tag{4}$$

Figure 5 shows temperature dependence of $C_0(T)$ of the $Gd_{55}Al_{20}Co_{20}Ni_5$ BMG. Thus, associated with the $(-\Delta S_m)$-T curves, we can obtain the $\Delta T_{ad} - T$ curve of the $Gd_{55}Al_{20}Co_{20}Ni_5$ BMG according to Eq. (4), as shown in Fig. 5. The peak value of ΔT_{ad} for the $Gd_{55}Al_{20}Co_{20}Ni_5$ BMG is about 4.74 K under 5 T, which is higher than any of the values for the BMGs previously reported.

As shown in Table I, we have found that the minor Ni substitution for Co in a $Gd_{55}Al_{20}Co_{25}$ glass forming alloy can obviously improve the MCE (including $-\Delta S_m^{peak}$ and RC) of the BMG. As is known, the MCE as well as the M_s is closely related to the total magnetic moment of a ferromagnetic material because either the entropy change with the variation of magnetic field or the magnetization process of these materials

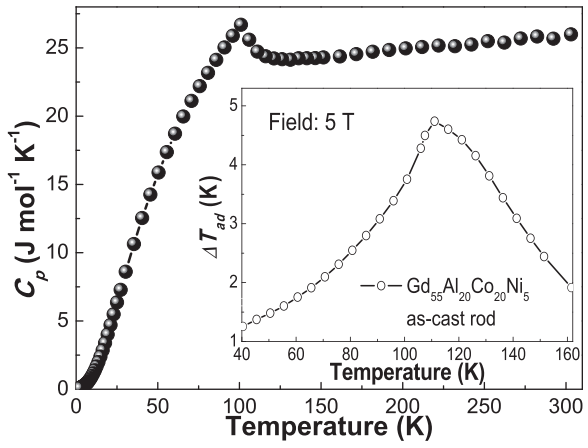

FIG. 5. Heat capacity of $Gd_{55}Al_{20}Co_{20}Ni_5$ BMG under the zero magnetic field, the inset the $\Delta T_{ad} - T$ curve of $Gd_{55}Al_{20}Co_{20}Ni_5$ BMG under 5 T.

depend mainly on the ordering of the magnetic moments. The nominal magnetic moment of the $Gd_{55}Al_{20}Co_{25}$ BMG is about 5.6 μ_B, and is about 5.52 μ_B for the $Gd_{55}Al_{20}Co_{20}Ni_5$ BMG. It is anomalous because the Ni addition will decrease the nominal magnetic moment but at the same time enhance the magnetic properties of the BMG. Considering the strong interaction of the magnetic moment between the rare-earth element with 4*f*-electrons and the transition metal element with 3*d*-electrons, the effective magnetic moment (μ_{eff}) was applied to evaluate the effect of minor element substitution on the magnetic properties of the BMGs. Plots of the ratio H/M as a function of temperature (H/M-T curve), derived from the M-T curves under 300 Oe for the $Gd_{55}Al_{20}Co_{20}Ni_5$ as well as $Gd_{55}Al_{20}Co_{25}$ as-cast rods, are shown in the inset of Fig. 2(b). Therefore, according to the Curie-Weiss law, μ_{eff} can be obtained from the H/M-T curves with values of about 7.63 μ_B for the $Gd_{55}Al_{20}Co_{20}Ni_5$ BMG and about 7.24 μ_B for the $Gd_{55}Al_{20}Co_{25}$ BMGs. Similar to the M_s value, μ_{eff} of the $Gd_{55}Al_{20}Co_{20}Ni_5$ glassy rod is also 5% larger than that of the $Gd_{55}Al_{20}Co_{25}$ rod. Moreover, we can also find that the effective magnetic moment of the $Gd_{55}Al_{20}Co_{20}Ni_5$ amorphous alloy is about 38% higher than the nominal one which, in contrast, is only 29% higher than the nominal one in the $Gd_{55}Al_{20}Co_{25}$ glassy alloy. Therefore, the minor Ni addition in the $Gd_{55}Al_{20}Co_{25}$ glass forming alloy as a replacement for Co obviously enhances the 3*d*-4*f* interaction, and this appears to be the mechanism for the improved magnetic properties by element substitution.

IV. CONCLUSIONS

In summary, we fabricated $Gd_{55}Al_{20}Co_{20}Ni_5$ BMG by copper mold casting through the minor substitution of Co with Ni in a $Gd_{55}Co_{25}Al_{20}$ glass forming alloy. The BMG shows a similar GFA to the $Gd_{55}Co_{25}Al_{20}$ glassy alloy and exhibits enhanced magnetic properties by the minor Ni addition. Magnetic measurements of the $Gd_{55}Al_{20}Co_{20}Ni_5$ as-cast rod have revealed values of $M_s = 217$ Am^2/kg under the field of 2 T, and $-\Delta S_m^{peak} = 9.8$ $Jkg^{-1}K^{-1}$, $RC_{HHW} = 615$ Jkg^{-1}, and $RC_A = 829$ Jkg^{-1} under the field of 5 T. All these values are higher than the values for most of other BMGs under the same magnetic field. The field dependence of $-\Delta S_m^{peak}$ roughly follows the $-\Delta S_m^{peak} \propto H^{0.85}$ relationship near T_c. The adiabatic temperature rise reached about 4.74 K under 5 T, which is higher than any of other BMGs previously reported. The improved magnetic properties of the $Gd_{55}Al_{20}Co_{20}Ni_5$ amorphous rod is most likely to be induced by the enlarged μ_{eff} by minor Ni substitution for Co, which means the enhanced interaction between the *3d* electron in Co and the *4f* electron in Gd.

ACKNOWLEDGMENTS

The work described in this paper was supported by the National Nature Science Foundation of China (Grant Nos. 51171100, 51001113, and 51271103) and the Research Grants Council of the Hong Kong Special Administrative Region, China (Project No. PolyU 511212).

[1]E. Warburg, Ann. Phys. **249**, 141 (1881).
[2]N. A. de Oliveira and P. J. von Ranke, Phys. Rep. **489**, 89 (2010).
[3]J. Glanz, Science **279**, 2045 (1998).
[4]V. K. Pecharsky and K. A. Gschneider, Jr., Phys. Rev. Lett. **78**, 4494 (1997).
[5]B. F. Yu, Q. Gao, B. Zhang, X. Z. Meng, and Z. Chen, Int. J. Refrig. **26**, 622 (2003).
[6]A. M. Tishin and Y. I. Spichkin, *The Magnetocaloric Effect and Its Applications* (Institute of Physics Publishing Ltd., Bristol, 2003).
[7]K. A. Gschneider, Jr., V. K. Pecharsky, and A. O. Tsokol, Rep. Prog. Phys. **68**, 1479 (2005).
[8]V. K. Pecharsky and K. A. Gschneider, Jr., J. Magn. Magn. Mater. **200**, 44 (1999).
[9]E. Brück, J. Phys. D: Appl. Phys. **38**, R381 (2005).
[10]O. Tegus, E. Brück, K. H. J. Buschow, and F. R. de Boer, Nature **415**, 150 (2002).
[11]L. Morellon, J. Blasco, P. A. Algarabel, and M. R. Ibarra, Phys. Rev. B **62**, 1022 (2000).
[12]V. K. Pecharsky and K. A. Gschneider, Jr., Appl. Phys. Lett. **70**, 3299 (1997).
[13]S. J. Kim, L. J. Lee, M. H. Jung, H. J. Oh, and Y. S. Kwon, J. Magn. Magn. Mater. **323**, 1094 (2011).
[14]A. Fujita, S. Fujieda, Y. Hasegawa, and K. Fukamichi, Phys. Rev. B **67**, 104416 (2003).
[15]F. X. Hu, B. G. Shen, J. R. Sun, and G. H. Wu, Phys. Rev. B **64**, 132412 (2001).
[16]H. Wada and Y. Tanabe, Appl. Phys. Lett. **79**, 3302 (2001).
[17]L. G. de Medeiros, Jr. and N. A. de Oliveira, J. Alloys Compd. **501**, 177 (2010).
[18]G. V. Brown, J. Appl. Phys. **47**, 3673 (1976).
[19]J. Sun, J. F. Wu, and J. R. Sun, J. Appl. Phys. **106**, 083902 (2009).
[20]Q. Luo, D. Q. Zhao, M. X. Pan, and W. H. Wang, Appl. Phys. Lett. **89**, 081914 (2006).
[21]L. Liang, X. Hui, Y. Wu, and G. L. Chen, J. Alloys Compd. **457**, 541 (2008).
[22]Q. Luo, D. Q. Zhao, M. X. Pan, and W. H. Wang, Appl. Phys. Lett. **92**, 011923 (2008).
[23]J. Du, Q. Zheng, Y. B. Li, Q. Zhang, D. Li, and Z. D. Zhang, J. Appl. Phys. **103**, 023918 (2008).
[24]L. Xia, K. C. Chan, and M. B. Tang, J. Alloys Compd. **509**, 6640 (2011).
[25]S. Lu, M. B. Tang, and L. Xia, Physica B **406**, 3398 (2011).
[26]D. Ding, L. Xia, Z. H. Yu, and Y. D. Dong, Chin. Phys. Lett. **25**, 3414 (2008).
[27]N. S. Bingham, H. Wang, F. Qin, H. X. Peng, J. F. Sun, V. Franco, H. Srikanth, and M. H. Phan, Appl. Phys. Lett. **101**, 102407 (2012).
[28]F. Yuan, J. Du, and B. Shen, Appl. Phys. Lett. **101**, 032405 (2012).
[29]J. Y. Law, V. Franco, and R. V. Ramanujan, Appl. Phys. Lett. **98**, 192503 (2011).
[30]V. Franco, J. M. Borrego, A. Conde, and S. Roth, Appl. Phys. Lett. **88**, 132509 (2006).
[31]Y. Liu, J. Zhang, Y. Wang, Y. Zhu, Z. Yang, J. Chen, and S. Cao, Appl. Phys. Lett. **94**, 112507 (2009).
[32]V. Franco, J. S. Blázquez, and A. Conde, Appl. Phys. Lett. **89**, 222512 (2006).
[33]M. H. Phan, V. Franco, A. Chaturvedi, S. Stefanoski, G. S. Nolas, and H. Srikanth, Phys. Rev. B **84**, 054436 (2011).
[34]S. Kallel, N. Kallel, O. Peña, and M. Oumezzine, J. Alloys Compd. **504**, 12 (2010).
[35]L. Xia, S. S. Fang, C. L. Jo, and Y. D. Dong, Intermetallics **14**, 1098 (2006).
[36]L. Xia, K. C. Chan, L. Liu, and G. Wang, J. Phys. D: Appl. Phys. **41**, 225410 (2008).